Electronic Supporting Information

Reversible single-crystal to single-crystal transformation between triangular single-molecule toroics

Lixi Feng,[a] Yue Yang,[a] Yu-Xia Wang,*[a,b] Yizheng Zhao,[a] Zhong-Yi Liu,[b] Junzhuang Cong,[c] Yi-Quan Zhang,[d] and Peng Cheng*[a]

[a] Department of Chemistry, Key Laboratory of Advanced Energy Materia Chemistry, Renewable Energy Conversion and Storage Center and Frontiers Science Center for New Organic Matter, and Haihe Laboratory of Sustainable Chemical Trans-formations (Tianjin), College of Chemistry, Nankai University, Tianjin 300071, China

[b] College of Chemistry, Tianjin Normal University, Tianjin, 300387, China

[C] Institute of Physics, Chinese Academy of Sciences, Beijing 100190, P. R. China.

[d] Jiangsu Key Lab for NSLSCS, School of Physical Science and Technology, Nanjing Normal University, Nanjing 210023, P. R. China

Contents

1. Experimental details

Materials and measurements

All reagents and solvents were commercially obtained and used as received without any further purification. Compound **1** was synthesized following the reported procedure. Put **1** in 30 mL of acetone at room temperature. Five days later, needle like crystals of **1** were converted into block ones of **2**.

Single-crystal X-ray diffraction was performed on an Agilent SuperNova diffractometer (120 K) equipped with graphite monochromate Mo-Kα radiation (α= 0.71073 Å). The structure is solved by direct methods and refined by the full matrix least-squares method on F^2 with anisotropic thermal parameters for all nonhydrogen atoms using the SHELXL program. Hydrogen atoms were located geometrically and refined isotopically.

Magnetic properties were measured on powder samples using a Quantum Design superconducting quantum interference device magnetometer.

The programs VASP 5.44, OpenMolcas, SINGLE_ANISO and POLY_ANISO are used for related calculations.

2. Magnetic characterization

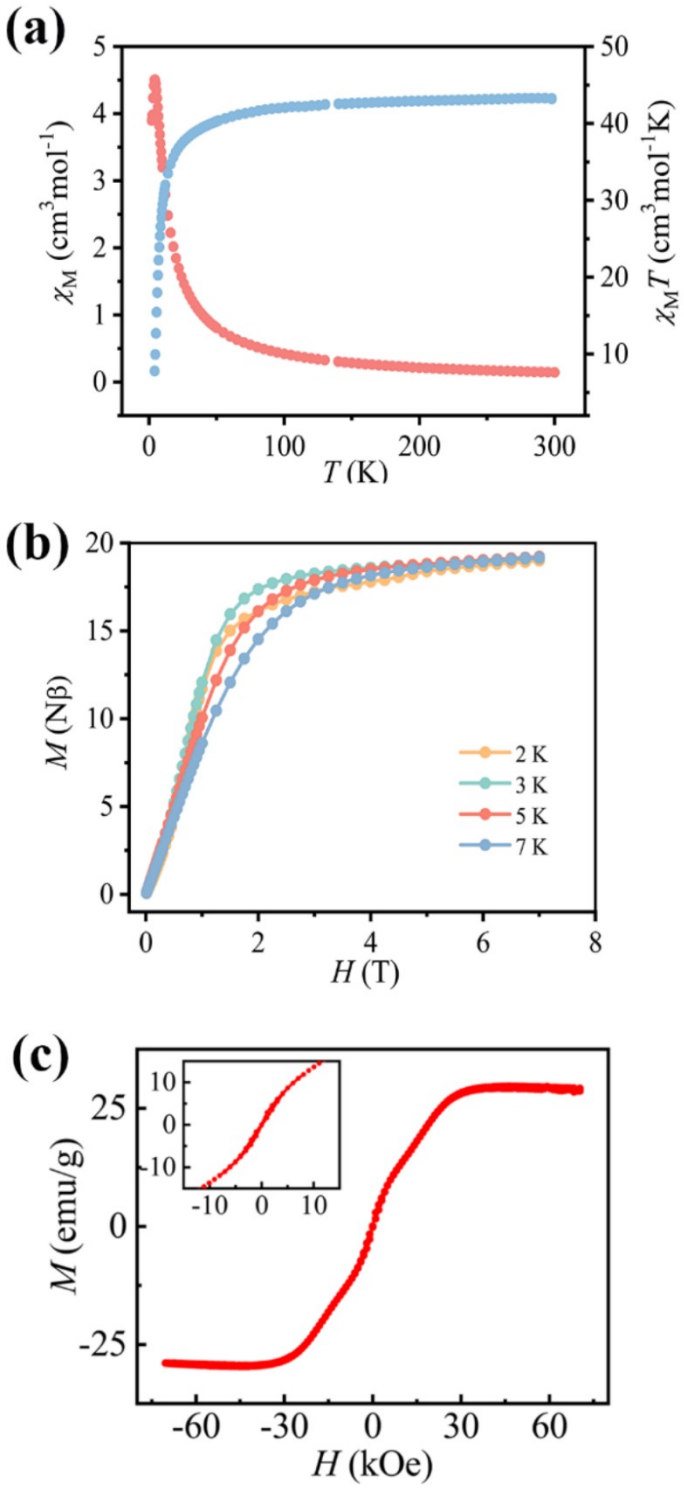

Fig. S1. DC magnetic measurements of powder and single crystal sample. (a) χ_M *vs*. *T* and $\chi_M T$ *vs. T* for **2** with an applied magnetic field of 0.1 T. (b) Field-dependent magnetization at 2-7 K. (c) The magnetic hysteresis loop of **2** at 2 K.

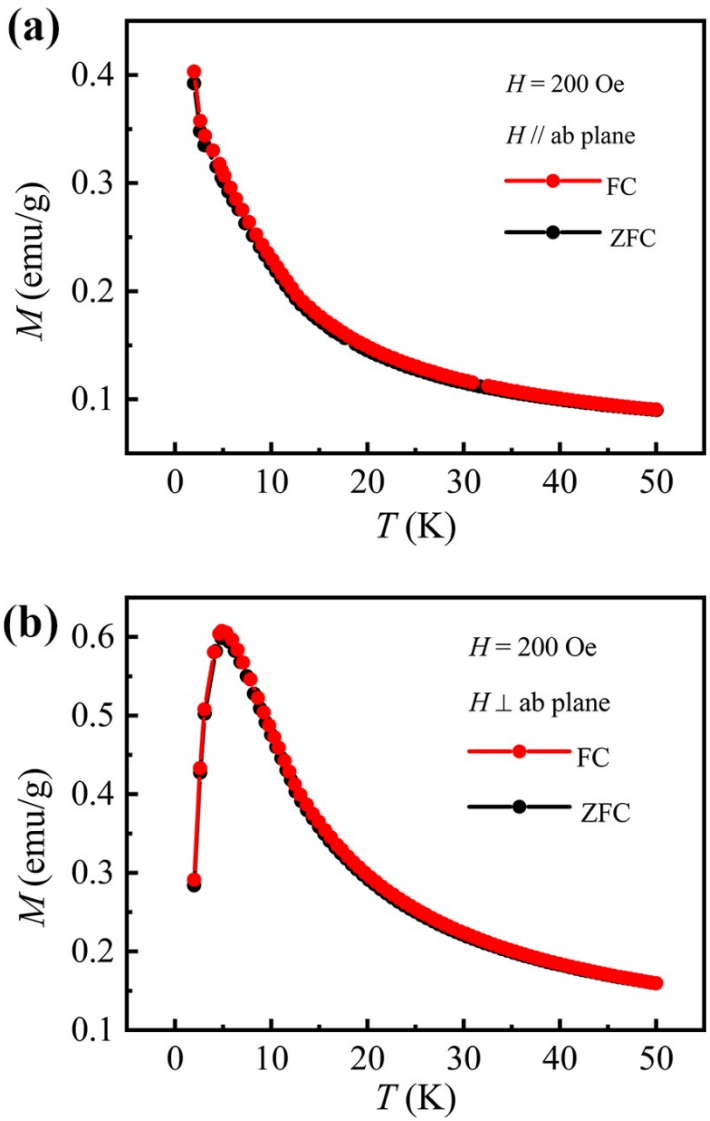

Fig. S2. Plots of zero field-cooled (black) and field-cooled (red) on a single-crystal sample of **2** under 200 Oe. Magnetic field were applied parallel (a) and perpendicular (b) to the ab plane.

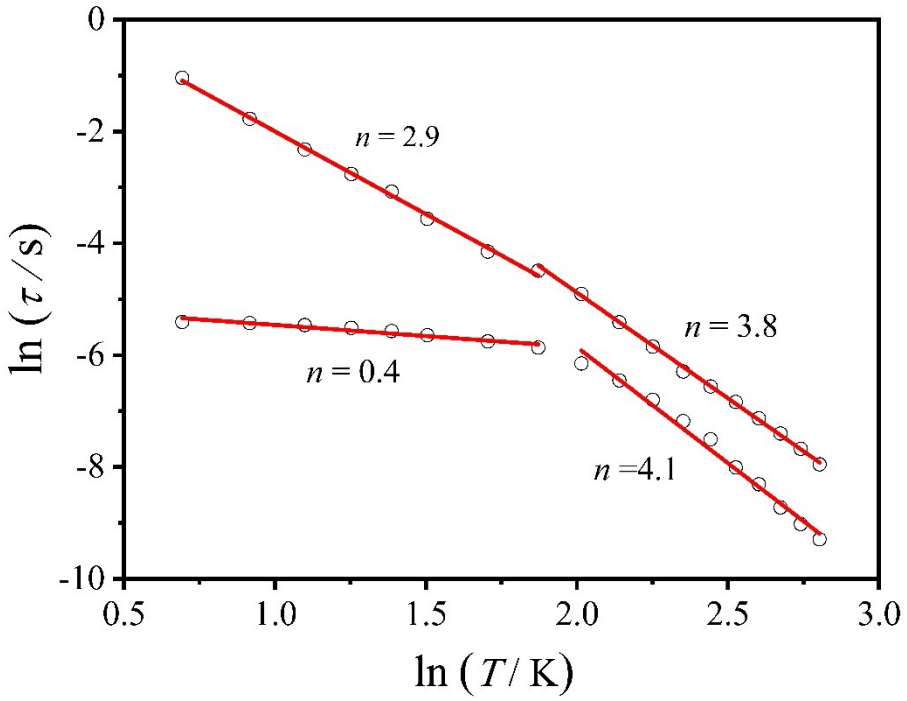

Fig. S3. Plots of ln(*τ*) *vs*. ln(*T*). The solid red lines represent the best fitting result.

3. Computational details

Compound **2** has three types of magnetic center Dy^{3+} ions indicated as **2_Dy1**, **2_Dy2** and **2_Dy3**. Complete-active-space self-consistent field (CASSCF) calculations on individual Dy^{3+} fragments for compound **2** (see Figure S1) on the basis of single-crystal X-ray determined geometry have been carried out with OpenMolcas[S1] program package. Each individual Dy^{3+} fragment in **2** was calculated keeping the experimentally determined structures of the corresponding compound while replacing the other Dy^{3+} ions with diamagnetic Lu^{3+}.

The basis sets for all atoms are atomic natural orbitals from the OpenMolcas ANO-RCC library: ANO-RCC-VTZP for Dy^{3+}; VTZ for close O and N; VDZ for distant atoms. The calculations employed the second order Douglas-Kroll-Hess Hamiltonian, where scalar relativistic contractions were taken into account in the basis set and the spin-orbit couplings were handled separately in the restricted active space state interaction (RASSI-SO) procedure.[S2–S3] Active electrons in 7 active orbitals include all *f* electrons (CAS (9 in 7) in the CASSCF calculation. To exclude all the doubts, we calculated all the roots in the active space. We have mixed the maximum number of spin-free state which was possible with our hardware (all from 21 sextets, 128 from 224 quadruplets, 130 from 490 doublets for Dy^{3+}). SINGLE_ANISO[S4–S6] program was used to obtain the energy levels, ***g*** tensors, magnetic axes, *et al.* based on the above CASSCF/RASSI-SO calculations.

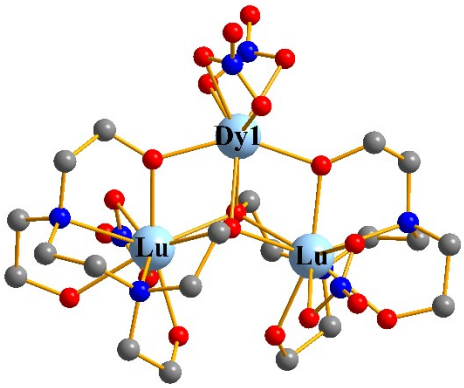

2_Dy1

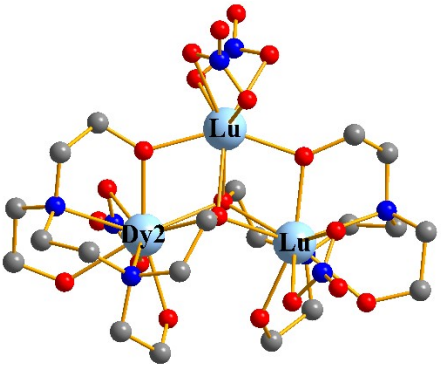

2_Dy2

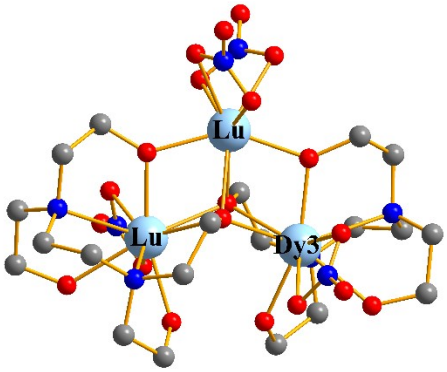

2_Dy3

Fig. S4. Calculated model structures of individual Dy^{3+} fragments in compound **2**; H atoms are omitted for clarify.

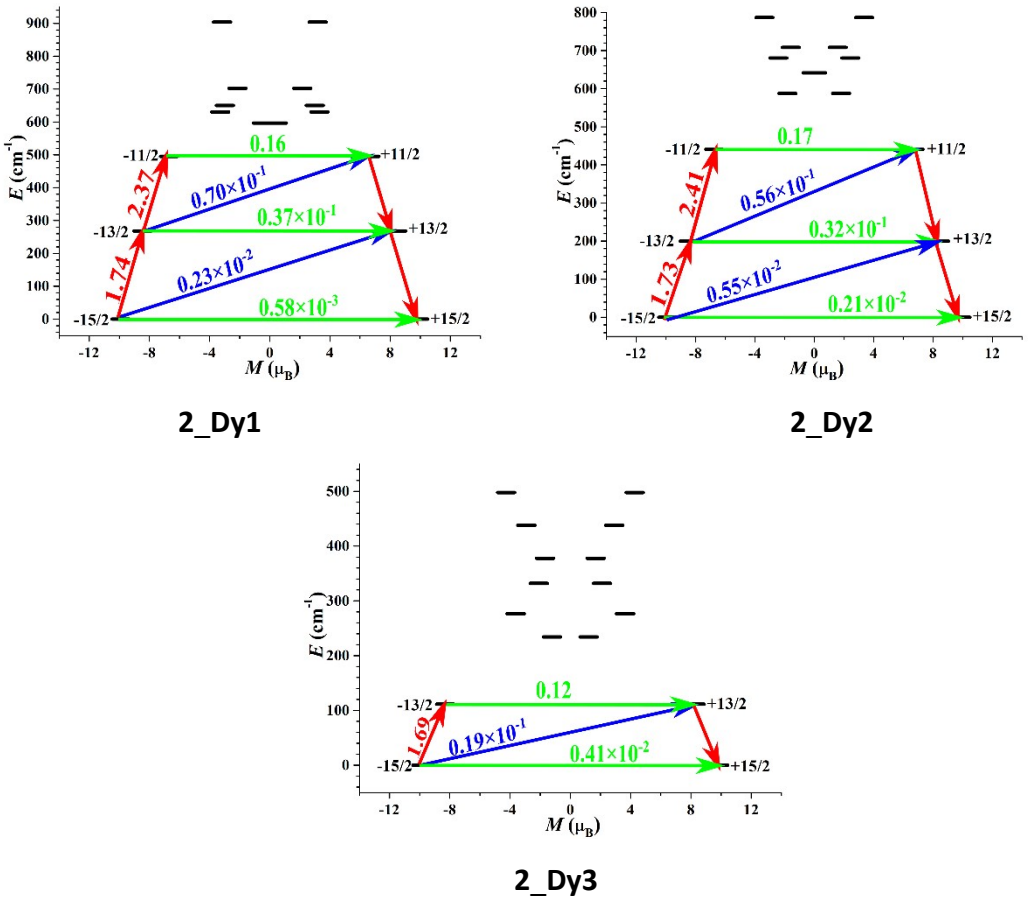

Fig. S5. Magnetization blocking barriers of individual Dy^{3+} fragments for compound **2**. The thick black lines represent the KDs as a function of their magnetic moment along the magnetic axis. The green lines correspond to diagonal quantum tunneling of magnetization (QTM); the blue line represent off-diagonal relaxation process. The numbers at each arrow stand for the mean absolute value of the corresponding matrix element of transition magnetic moment.

To fit the exchange interactions in compound **2**, we took two steps to obtain it. Firstly, we calculated individual Dy^{3+} fragments using CASSCF/RASSI-SO to obtain the corresponding magnetic properties. Then, the exchange interaction between the magnetic centers was considered within the Lines model, [S7] while the account of the dipole-dipole magnetic coupling was treated exactly. The Lines model is effective and has been successfully used widely in the research field of *d* and *f*-elements single-molecule magnets. [S8- S9]

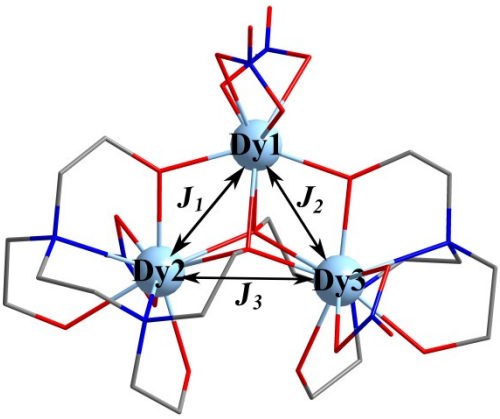

Fig. S6. Scheme of the Dy^{3+}-Dy^{3+} interactions in compound **2**.

For compound **2**, there are three types of $\tilde{J}$. The Ising exchange Hamiltonian is:

$$\hat{H}_{exch} = -\tilde{J}_1\hat{S}_{Dy1}\hat{S}_{Dy2} - \tilde{J}_2\hat{S}_{Dy1}\hat{S}_{Dy3} - \tilde{J}_3\hat{S}_{Dy2}\hat{S}_{Dy3} \qquad \text{(S1)}$$

The $\tilde{J}_1 = 25\cos\varphi J_1$, where φ is the angle between the anisotropy axes on sites Dy1 and Dy2, and J_1 is the corresponding Lines exchange coupling parameter. The other two interactions $\tilde{J}_2$ and $\tilde{J}_3$ also have similar expressions. The $\tilde{S}_{Dy}$ = 1/2 is the ground pseudospin on the Dy^{3+} site. $\tilde{J}_{total}$ is the parameter of the total magnetic interaction ($\tilde{J}_{total} = \tilde{J}_{dipolar} + \tilde{J}_{exchange}$) between magnetic center ions. The dipolar magnetic coupling can be calculated exactly, while the exchange coupling constant was fitted through comparison of the computed and measured magnetic susceptibilities using POLY_ANISO program.[S4-S6]

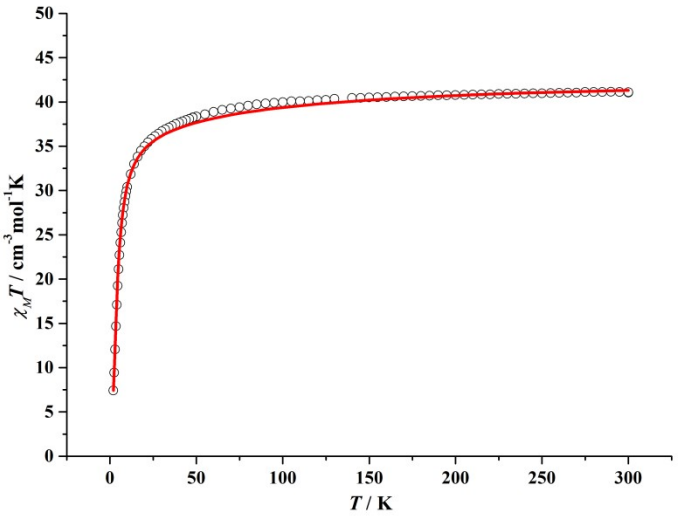

Fig. S7. Calculated (red solid line) and experimental (black square dot) data of magnetic susceptibilities of **2**. The intermolecular interaction zJ' of compound **2** was fitted to 0.02 cm^{-1}.

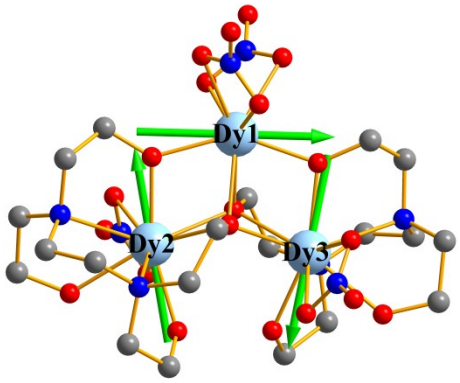

Fig. S8. Calculated orientations of the local main magnetic axes on Dy^{3+} ions of compound **2** in the ground KDs.

4. Tables

Table S1. Summary of space groups and cell parameters at 120 K.

CCDC	2290194
T (K)	120K
Formular	$C_{23}H_{49}Dy_3N_8O_{21}$
Space group	$\bar{P}1$
a (Å)	11.8703(8)
b (Å)	11.8756(9)
c (Å)	15.4895(7)
α (deg.)	102.276(5)
β (deg.)	107.969(5)
γ (deg.)	100.557(6)
V(Å^3)	1955.4(2)
Z	2
Dc (g·cm^{-3})	2.142
μ (mm^{-1})	5.762
R_{int}	0.0559
GOOF	1.121
[a]R_1	0.0694
[b]wR_2	0.1575
$\triangle\rho_{max}$ (e Å^{-3})	4.6
$\triangle\rho_{min}$ (e Å^{-3})	-2.5

[a] $R_1 = \sum||Fo| - |Fc||/\sum|Fo|$; [b] $wR_2 = [\sum w(Fo^2 - Fc^2)^2/\sum w(Fo^2)^2]^{1/2}$.

Table S2 Continuous shape measure calculations for the Dy^{3+} ions for **2**.

2			
Dy^{3+}	Dy1 [ML_8]	Dy2 [ML_9]	Dy3 [ML_9]
Structure	D_{4d}	C_{4v}	C_{4v}
Deviation value	3.116	2.369	2.221

D_{4d} = Square antiprism (SAPR-8); C_{4v} = Capped square antiprism J10 (JCSAPR-9)

Table S3. The best fitting results of the temperature-dependent relaxation times.

$\tau^{-1} = C + BT^n + \tau_0^{-1} \exp(-U_{eff}/k_BT)$		
	faster	slower
C	---	262.94
B	0.40	---
n	---	---
τ_0	9.8×10^{-6}	3.0×10^{-6}
U_{eff} (cm^{-1})	72.0	59.0
dominated relaxation processes	Raman + Orbach	QTM + Orbach

Table S4. Calculated energy levels (cm^{-1}), ***g*** (g_x, g_y, g_z) tensors and predominant m_J values of the lowest eight Kramers doublets (KDs) of individual Dy^{3+} fragments for compound **2** using CASSCF/RASSI-SO with OpenMolcas.

KDs	**2_Dy1**			**2_Dy2**			**2_Dy3**		
	E	***g***	m_J	*E*	***g***	m_J	*E*	***g***	m_J
1	0.0	0.001 0.001 19.835	±15/2	0.0	0.006 0.006 19.831	±15/2	0.0	0.010 0.014 19.761	±15/2
2	268.1	0.108 0.117 16.998	±13/2	200.0	0.089 0.102 17.086	±13/2	111.1	0.359 0.377 16.988	±13/2
3	495.3	0.261 0.673 13.439	±11/2	440.6	0.382 0.676 13.638	±11/2	233.9	0.499 1.881 13.525	±1/2
4	596.8	0.949 1.934 15.003	±1/2	587.4	3.597 4.410 11.293	±9/2	276.5	1.132 3.327 7.753	±11/2
5	630.3	0.389 2.133 11.143	±3/2	641.6	11.620 5.857 0.017	±1/2	331.9	9.056 5.584 0.918	±3/2
6	650.1	2.256 5.744 10.976	±9/2	680.8	0.685 2.905 8.158	±9/2	377.8	1.410 4.143 11.727	±7/2
7	702.2	0.641 1.445 15.218	±7/2	708.4	1.637 4.801 10.255	±5/2	438.0	6.749 5.862 2.263	±9/2
8	903.9	0.088 0.092 19.515	±7/2	787.0	1.135 2.566 16.216	±7/2	497.9	1.266 3.878 15.053	±7/2

Table S5. Wave functions with definite projection of the total moment | m_J > for the lowest eight KDs of individual Dy^{3+} fragments for **2**.

	E/cm^{-1}	wave functions
2_Dy1	0.0	99.5%|±15/2>
	268.1	97.2%|±13/2>
	495.3	87.3%|±11/2>+3.8%|±9/2>
	596.8	65.0%|±1/2>+13.9%|±3/2>+9.3%|±9/2>+8.4%|±5/2>
	630.3	37.7%|±3/2>+34.2%|±9/2>+16.9%|±5/2>+8.7%|±7/2>
	650.1	25.5%|±9/2>+24.3%|±3/2>+23.1%|±7/2>+14.1%|±5/2>+12.1%|±1/2>
	702.2	39.3%|±7/2>+37.6%|±5/2>+10.4%|±9/2>+6.0%|±3/2>
	903.9	26.2%|±7/2>+21.8%|±5/2>+16.2%|±3/2>+16.1%|±9/2>+13.1%|±1/2>
2_Dy2	0.0	99.4%|±15/2>
	200.0	96.4%|±13/2>
	440.6	84.5%|±11/2>+6.6%|±9/2>
	587.4	27.5%|±9/2>+26.0%|±1/2>+23.1%|±3/2>+9.4%|±7/2>+9.2%|±5/2>
	641.6	65.0%|±1/2>+16.4%|±3/2>+9.9%|±9/2>
	680.8	34.9%|±9/2>+32.0%|±3/2>+21.2%|±7/2>+5.2%|±1/2>
	708.4	54.0%|±5/2>+24.8%|±3/2>+14.0%|±7/2>
	787.0	51.9%|±7/2>+26.6%|±5/2>+16.2%|±9/2>
2_Dy3	0.0	98.7%|±15/2>
	111.1	89.8%|±13/2>
	233.9	48.8%|±1/2>+24.5%|±3/2>+17.5%|±11/2>
	276.5	41.5%|±11/2>+15.7%|±1/2>+13.4%|±9/2>+12.2%|±5/2>12.2%|±3/2>
	331.9	30.1%|±3/2>+22.3%|±1/2>+14.6%|±5/2>+14.4%|±11/2>+9.8%|±9/2>
	377.8	33.8%|±7/2>+22.8%|±5/2>+18.6%|±3/2>+14.1%|±9/2>+4.0%|±1/2>
	438.0	33.2%|±9/2>+25.2%|±5/2>+12.1%|±11/2>+11.4%|±7/2>+8.7%|±3/2>
	497.9	44.5%|±7/2>+26.9%|±9/2>+18.5%|±5/2>+5.2%|±3/2>

Table S6. Exchange energies E (cm^{-1}), the transversal magnetic moments Δ_t (μ_B) and the main values of the g_z for the lowest four exchange doublets of compound **2**.

	2		
	E	Δ_t	g_z
1	0.0	5.986×10^{-11}	12.578
2	5.4	1.570×10^{-8}	43.949
3	5.6	2.238×10^{-8}	43.417
4	6.0	5.349×10^{-9}	27.093

Table S7. Angles between the main magnetic axes on Dy^{3+} ions in their ground KDs and the angles between the magnetic axes and the Dy_3 plane for **2**.

	2			
Dy^{3+} sites	Dy1	Dy2	Dy3	Dy_3 plane
Dy1	0°	101.4°	99.7°	−6.2°
Dy2	101.4°	0°	158.8°	−2.5°
Dy3	99.7°	158.8°	0°	4.3°

Table S8. Fitted exchange couplings $\tilde{J}_{exch}$, the calculated dipole-dipole interactions $\tilde{J}_{dip}$ and the total constants $\tilde{J}_{total}$ between magnetic center ions in **2** (cm^{-1}). The intermolecular interaction *zJ´* of **2** was fitted to 0.02 cm^{-1}.

	$\tilde{J}_{exch}$	$\tilde{J}_{dip}$	$\tilde{J}_{total}$
J_1	−0.49	−5.37	−5.86
J_2	−0.84	−5.73	−6.57
J_3	−2.33	−2.81	−5.14

5. References

S1 I. F. Galván, M. Vacher, A. Alavi, C. Angeli, F. Aquilante, J. Autschbach, J. J. Bao, S. I. Bokarev, N. A. Bogdanov, R. K. Carlson, L. F. Chibotaru, J. Creutzberg, N. Dattani, M. G. Delcey, S. S. Dong, A. Dreuw, L. Freitag, L. M. Frutos, L. Gagliardi, F. Gendron, A. Giussani, L. González, G. Grell, M. Y. Guo, C. E. Hoyer, M. Johansson, S. Keller, S. Knecht, G. Kovacevic, E. Källman, G. L. Manni, M. Lundberg, Y. J. Ma, S. Mai, J. P. Malhado, P. Å. Malmqvist, P. Marquetand, S. A. Mewes, J. Norell, M. Olivucci, M. Oppel, Q. M. Phung, K. Pierloot, F. Plasser, M. Reiher, A. M. Sand, I. Schapiro, P. Sharma, C. J. Stein, L. K. Sørensen, D. G. Truhlar, M. Ugandi, L. Ungur, A. Valentini, S. Vancoillie, V. Veryazov, Q. Weser, T. A. Wesołowski, Per-Olof. Widmark, S. Wouters, A. Zech, J. P. Zobel and R. Lindh, *J. Chem. Theory Comput*., 2019, **15**, 5925–5964.

S2 P. Å Malmqvist, B. O. Roos and B. Schimmelpfennig, *Chem. Phys. Lett.,* 2002, **357**, 230–240.

S3 B. A. Heß, C. M. Marian, U. Wahlgren and O. Gropen, *Chem. Phys. Lett.*, 1996, **251**, 365–371.

S4 L. F. Chibotaru, L. Ungur and A. Soncini, *Angew. Chem., Int. Ed.,* 2008, **47**, 4126–4129.

S5 L. Ungur, W. Van den Heuvel and L. F. Chibotaru, *New J. Chem.,* 2009, **33**, 1224–1230.

S6 L. F. Chibotaru, L. Ungur, C. Aronica, H. Elmoll, G. Pilet and D. Luneau, *J. Am. Chem. Soc.,* 2008, **130**, 12445–12455.

S7 M. E. Lines, *J. Chem. Phys*., 1971, **55**, 2977−2984.

S8 K. C. Mondal, A. Sundt, Y. H. Lan, G. E. Kostakis, O. Waldmann, L. Ungur, L. F. Chibotaru, C. E. Anson and A. K. Powell, *Angew. Chem., Int. Ed.,* 2012, **51**, 7550−7554.

S9 S. K. Langley, D. P. Wielechowski, V. Vieru, N. F. Chilton, B. Moubaraki, B. F. Abrahams, L. F. Chibotaru and K. S. Murray, *Angew. Chem., Int. Ed.,* 2013, **52**, 12014–12019.